PHYSICAL REVIEW LETTERS

Articles published week ending 25 OCTOBER 2013

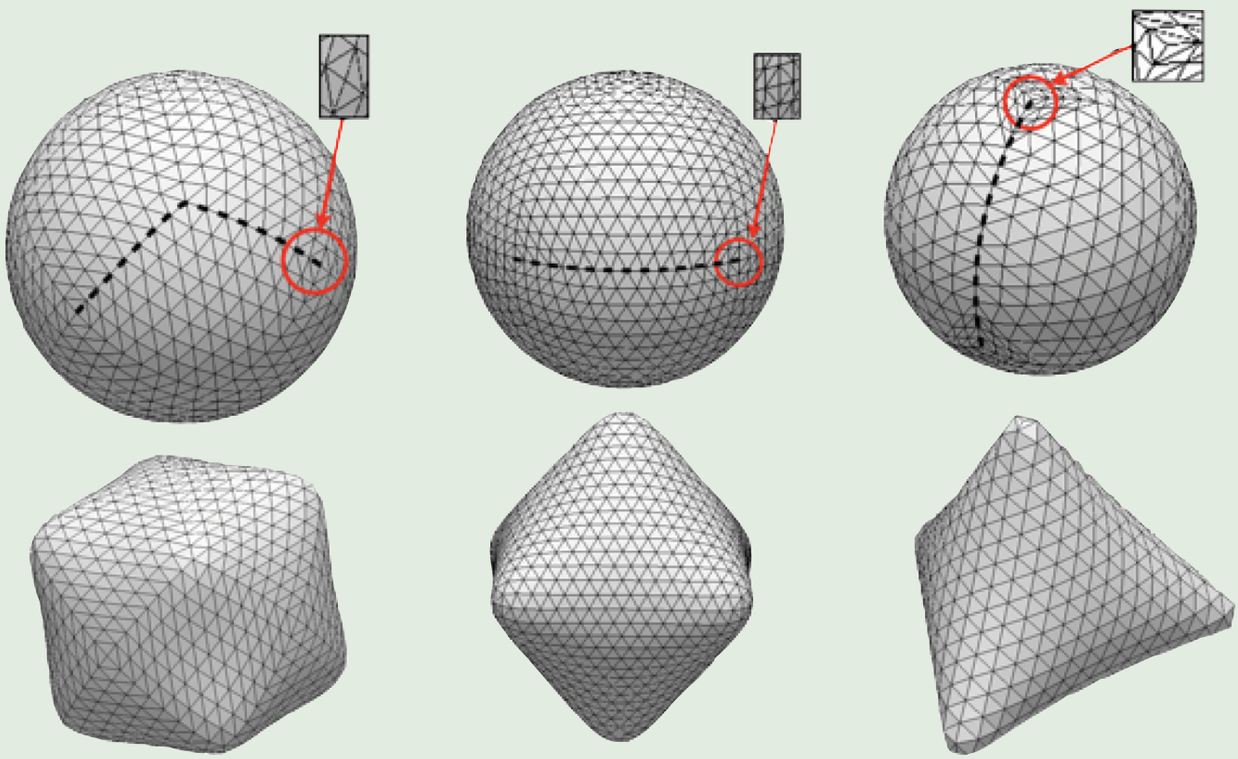

Published by
American Physical Society

APS physics

Volume 111, Number 17

Elastic Platonic Shells

Ee Hou Yong,[1] David R. Nelson,[1,2] and L. Mahadevan[1,2,*]

[1]*Department of Physics, Harvard University, Cambridge, Massachusetts 02138, USA*
[2]*School of Engineering and Applied Sciences, Harvard University, Cambridge, Massachusetts 02138, USA*

(Received 28 May 2013; published 23 October 2013)

On microscopic scales, the crystallinity of flexible tethered or cross-linked membranes determines their mechanical response. We show that by controlling the type, number, and distribution of defects on a spherical elastic shell, it is possible to direct the morphology of these structures. Our numerical simulations show that by deflating a crystalline shell with defects, we can create elastic shell analogs of the classical platonic solids. These morphologies arise via a sharp buckling transition from the sphere which is strongly hysteretic in loading or unloading. We construct a minimal Landau theory for the transition using quadratic and cubic invariants of the spherical harmonic modes. Our approach suggests methods to engineer shape into soft spherical shells using a frozen defect topology.

DOI: 10.1103/PhysRevLett.111.177801 PACS numbers: 64.60.Bd, 46.35.+z, 46.70.De

The continuum theory of elastic shells is applicable to the study of the mechanical response of systems across a wide range of length scales, from viruses (25 nm), vesicles (1 μm) [1,2], pollen grains (10–100 μm) [3], armored bubbles (10–100 μm) [4] to the behavior of macroscopic shells seen in aircraft fuselages (10 m) and even megascale lithospheric dynamics [5]. While the only geometric parameter in the study of these systems is their size-to-thickness ratio (which also translates into the only material parameter as well), on microscopic scales, the effects of crystallinity and defects may be important in determining the mechanical response of these shells. Indeed, isolated fivefold disclinations in flexible membranes with internal crystalline order are responsible for the buckling of a flat membrane [6], an effect that manifests itself in the distinctive icosahedral structure of virus capsids (100 nm) [7–9], the shape of colloidal shells [10], etc. To study these systems where crystallinity is potentially important, we need to account for the dynamics of the defects while simultaneously following the dynamics of the embedding shell, which might engender new defects. The two extreme limits correspond to the cases when the topography is frozen, but the defects are mobile [11–13], and the case when then the defects are frozen but the topography is mobile [8,9]. We focus here on the latter case, and show that by playing with the number, type, and arrangement of defects on a soft spherical shell, and then deflating it, we can derive controllable morphologies that resemble the platonic solids.

For crystalline complete spherical shells, topological considerations pose constraints that dictate that the number and type of disclinations must satisfy the condition known as Euler's formula, $\sum_z (6-z)N_z = \sum_z q_z N_z = 12$ [14], where N_z is the number of vertices with z-coordination number and $q_z = 6 - z$ is the topological charge of a vertex, as shown in the examples in Fig. 1(a). We assume that the core energies of disclinations are large so that a crystalline shell prefers to have the minimum number of isolated disclinations that satisfy Euler's formula and denote the number of three-, four-, and fivefold disclinations by $\vec{n} = \{n_3, n_4, n_5\}$; e.g., $\{0, 6, 0\}$ refers to a shell with six fourfold disclinations; a regular octahedron is an especially simple example. There are a total of 19 different possibilities that satisfy Euler's formula and they fall into three distinct universality classes [14]. We will further assume that the set of disclinations obeys some group symmetry G; i.e., the set of topological defects is invariant under the action of group G. Then, $\vec{n}$ and G maps any spherical surface with defects onto a unique polyhedron (many-to-one map) and henceforth, we will identify each surface with the corresponding polyhedron. The shape of the deformed shell depends sensitively on the thickness of the shell h, the radius of the shell R, and the average vertex spacing a from which we can form two dimensionless parameters h/R (aspect ratio), which characterizes the slenderness of the shell and R/a (lattice ratio) which characterizes the discreteness of the shell.

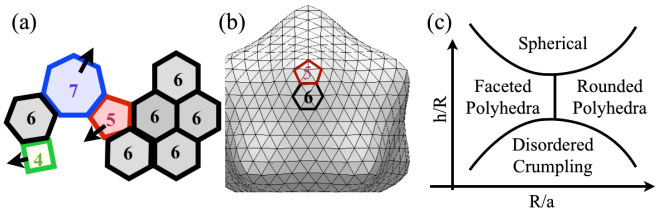

FIG. 1 (color online). Difference between frozen topography and frozen defects. (a) Frozen topography: There is a fourfold (green square), a fivefold (red pentagon), and a sevenfold disclination (blue heptagon) that are free to move on a fixed surface composed of sixfold sites (gray hexagons), often at the expense of creating additional defects [12]. (b) Frozen defects: The defects are frozen and the shape of the shell can freely change. (c) Phase diagram of buckled membranes as function of h/R and R/a.

We drive the formation of the polyhedral morphologies of these thin spherical shells by deflating them gradually [15]. This naturally leads to shapes that minimize the total energy of a thin two-dimensional shell that is the sum of the stretching energy and the bending energy, i.e., $U_T = U_S + U_B$ [16]. Because of the slenderness of the shell, it is energetically favorable to bend rather than to stretch, resulting in a highly faceted shape [17] from which the energy, which is initially smoothly distributed, becomes more and more nonuniform, with high energy concentrated in the bent regions (edges and vertices). Owing to the geometrical nonlinearity of the resulting energy densities, we used a numerical approach to determine the morphologies using SURFACE EVOLVER [18]. We construct a spherical shell with crystalline order containing a certain set of fixed defects of different types that satisfy Euler's formula and then decrease the volume in small decrements and equilibrate the elastic energy in each step. We find that beyond a critical decrement in the volume, the shell buckles into different faceted shapes such as that shown in Fig. 1(b); the specific form is constrained by the number, type, and orientation of the defects in the original spherical shell. As we vary the aspect ratio h/R, we find that thick spheres ($h/R \gtrsim 0.1$) deform isotropically and the shell is always smooth with no noticeable faceting; thin spherical shells tend to buckle into highly faceted structures. On the other hand, at low lattice ratio R/a, we generally get simpler buckled structures since there are fewer degrees of freedom; as we increase R/a, we get more complicated structures. At intermediate values of h/R and R/a, we get structures that resemble regular polyhedra [19]. In general, we expect to see various morphologies as a function of the two geometrical parameters corresponding to the aspect ratio and the lattice ratio as schematized in Fig. 1(c) [14]. In this Letter, we will consider $R/a \lesssim 10$ since at large lattice ratio, grain boundary scars become important [11,20].

In Fig. 2, we see that all shells corresponding to platonic solids arise as a function of the nature, number, and location of the defects on a sphere. Limiting ourselves to the case of a single class of defects, we use the classical Caspar-Klug notation (P, Q) [7], where $P, Q \in \mathbb{N}$. Thus, for $\vec{n} = \{0, 0, 12\}$ and $(P, 0)$, we get an icosahedron shell; for $\vec{n} = \{0, 0, 12\}$ and (P, P), we get its dual dodecahedron shell; for $\vec{n} = \{0, 6, 0\}$ and $(P, 0)$, we get an octahedron shell; for $\vec{n} = \{0, 6, 0\}$ and (P, P) we get its dual cube shell and finally $\vec{n} = \{4, 0, 0\}$ and $(P, 0)$, yields a tetrahedron shell. We can analyze the shapes of the buckled shells quantitatively by looking at the spherical harmonic expansion of the shape as characterized by the position of the vertices [8,21,22]

$$D(\theta, \phi) = \sum_{i=1}^{N} R_i \delta(\phi - \phi_i)\delta(\cos\theta - \cos\theta_i) \approx \sum_{\ell=0}^{L} \sum_{m=-\ell}^{\ell} a_\ell^m Y_\ell^m(\theta, \phi), \quad (1)$$

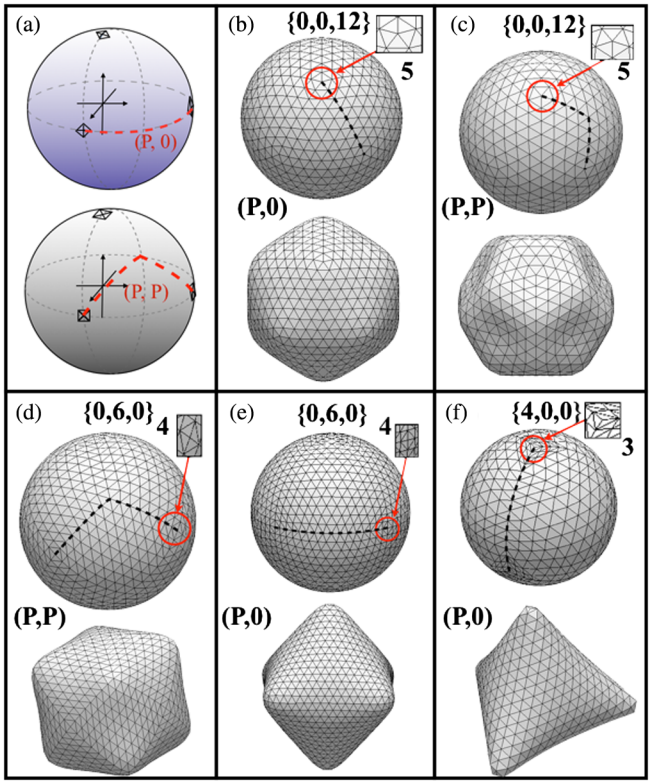

FIG. 2 (color online). (a) Difference between $(P, 0)$ and (P, P) shells illustrating the importance of the orientation of defects relative to the crystallographic axes. (b)–(d) Simulations of crystalline shells with different topological defects. The black dotted line shows the path between two disclinations and the number indicates the coordination number. The top (bottom) panel of each box denotes the initial (final) state. The final state is at volume fraction ≈ 0.8. (b) Icosahedron shell. (c) Dodecahedron shell. (d) Cube shell. (e) Octahedron shell. (f) Tetrahedron shell.

where (θ_i, ϕ_i, R_i) represents the polar coordinates of vertex i $(i = 1, \ldots N)$. Since a_ℓ^m's are coordinate dependent, we consider rotationally invariant quantities formed from a_ℓ^m's that measure the angular projection onto the different ℓ's [21,22]. Two such quantities are

$$Q_\ell = \frac{1}{a_0^0}\left(\frac{1}{2\ell + 1}\sum_{m=-\ell}^{\ell} |a_\ell^m|^2\right)^{1/2} \quad (2)$$

and

$$W_\ell = \frac{\sum_\Omega \begin{pmatrix} \ell & \ell & \ell \\ m_1 & m_2 & m_3 \end{pmatrix} a_\ell^{m_1} a_\ell^{m_2} a_\ell^{m_3}}{(\sum_m |a_\ell^m|^2)^{3/2}}, \quad (3)$$

where Ω denotes the set of m's such that $m_1 + m_2 + m_3 = 0$ and the parenthesis term in Eq. (3) is the Wigner $3j$ symbol. These parameters allow us to carry out a "shape spectroscopy." For example, Q_ℓ with $\ell > 0$ measures the asphericity of the shell; Q_4 measures tetrahedral or cubic

symmetry and Q_6 is an icosahedral order parameter [22–24], while W_ℓ measures the orientational symmetry type of the buckled membrane; W_4 and W_8 vanish for icosahedra and dodecahedra, and have different relative weights for the other platonic solids. They are normalized such that their magnitude is invariant to overall rescaling in a_ℓ^m's and $Q_0 = W_0 = 1$. In general, for a crystalline shell, we can evaluate its orientational symmetry by evaluating Q_ℓ/W_ℓ's and then compare them with the Q_ℓ/W_ℓ's of the corresponding platonic solid, for which the spherical harmonic representation can be calculated using known algebraic formulas [25]. The initial crystalline shell has nearly perfect spherical symmetry, i.e., $Q_\ell \approx \delta_{\ell,0}$. However, as the membrane buckles, the deformed shell starts to take on interesting shapes, with nonvanishing Q_ℓ's for $\ell > 0$. We calculate the Q_ℓ's for the various buckled crystalline shells in Fig. 2. The buckled icosahedron shell and dodecahedron shell have nonzero spherical harmonics only for $\ell = 0, 6, 10, 12, \ldots$; the cube shell and octahedron shell have nonvanishing spherical harmonics for $\ell = 0, 4, 6, 8, 10, \ldots$; the tetrahedron shell has $\ell = 0, 3, 4, 6, 7, 8, 9, 10, \ldots$.

Despite their rather different shapes, we find that the icosahedron shell and dodecahedron shell have identical magnitudes of W_ℓ's, as they belong to the same symmetry group G and these parameters characterize the symmetry of the vertices. We also compare the set of $|W_\ell|$'s of the buckled shells with their values for the ideal platonic solids as shown in Table I. In the case of the icosahedron shell and dodecahedron shell, we find that the first two nonzero W_ℓ's are $|W_6| = 0.1697$ and $|W_{10}| = 0.0940$; furthermore $(a_6^0)^2 = (11/7)|a_6^{\pm 5}|^2$, with all the other a_6^m vanishing, coefficients which maximize $|W_6|$ [22–24]. Similarly, for the cube shell and octahedron shell, we find that $(a_4^0)^2 = (14/5)|a_4^{\pm 4}|^2$, with all other $a_4^m = 0$, coefficients which maximize $|W_4|$ [22–24]. For the self-dual tetrahedron W_3 vanishes even though $Q_3 \neq 0$ [26]. Our analysis of the numerical simulations shows that the simplest shape parameters Q_ℓ and W_ℓ for the 5 platonic shells converge to that of the actual platonic solids. Thus, as long as the crystalline shell has frozen defects, this symmetry leads to buckled shapes with the same symmetry.

Having considered the symmetry of the buckled shells, we now consider their mechanical response as they buckle, focusing our attention on the $(P, 0)$ icosadeltahedral shell [8,9] which deforms into an icosahedral structure first. We focus on the case $(P, 0) = (8, 0)$, although the behavior for $P \lesssim 10$ is similar. On isotropic compression of a hollow spherical shell, it buckles and becomes faceted into an increasingly icosahedral shape, until eventually, at a scaled upper critical buckling pressure $p_b^u \approx 210$, the shell collapses abruptly into a structure with the symmetry of a squashed cube shown in Fig. 3. A transition from an icosahedral to squashed cubic symmetry is plausible, because an icosahedron can be dissected into three orthogonal golden rectangles [27]. The snap-through transition presumably selects one of five equivalent dissections and then squashes along one of the three orthogonal directions. Classical continuum elastic theory shows that the buckling pressure of an ideal sphere under hydrostatic pressure is $p_b^c = 4\sqrt{\kappa Y}/R^2 \approx 230$ [28], surprisingly close

TABLE I. Normalized invariant W_ℓ for the platonic solids.

Type	W_4	W_6	W_8	W_{10}
Icosahedron	⋯	−0.1697	⋯	+0.0940
Dodecahedron	⋯	+0.1697	⋯	−0.0940
Cube	−0.1593	+0.0132	+0.0584	−0.0901
Octahedron	+0.1593	−0.0132	+0.0584	−0.0901
Tetrahedron	+0.1593	+0.0132	+0.0584	−0.0901

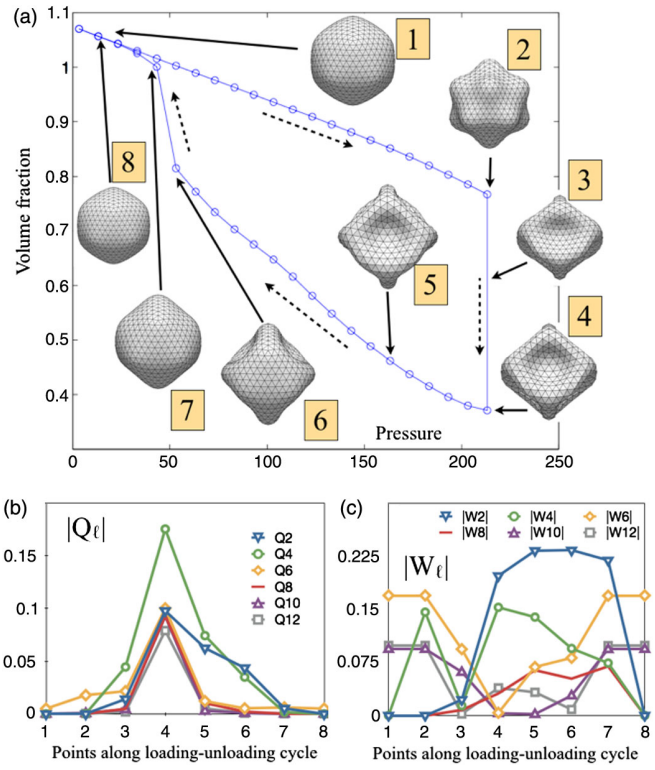

FIG. 3 (color online). (a) Mechanical response of a crushed icosahedral shell during the loading or unloading (LU) cycle. The labels (1) to (8) show the shape of the shell at different points during the LU cycle. As the pressure is gradually increased, the shell becomes more undulating as reflected in (2). At the upper critical buckling pressure $p_b^u \approx 210$, the icosahedral-like shell undergoes an abrupt collapse into a cubelike shell in (4). As the pressure is decreased, the shell does not return to the inflated condition by the same path at the pressure-volume diagram, but slowly inflates via a different pathway as reflected by Eqs. (6) and (7). The dotted arrows denote the direction of the LU cycle. (b) Plot of Q_ℓ during the LU cycle. We see significant deviation from icosahedral symmetry and the emergence of octahedral symmetry. The asymmetry of the curves about point 4 reflects the hysteretic behavior of the system. (c) Plot of $|W_\ell|$ during the LU cycle.

to our simulation results despite differing from the continuum theory in two important ways: our shells are crystalline and have topological defects. These two features evidently partially compensate. Next, we reduce the ambient pressure and we find that the shell remains cubelike with the six bulges becoming less pronounced, until eventually, at a lower critical pressure $p_b^l \approx 50$, the bulges pop back out and the shell recovers its icosahedral shape (see Fig. 3). Thus we see a strongly hysteretic transition in the morphology of these platonic shells as a function of pressure (or volume) in our simulations [29].

Quantitatively, as the shell becomes highly buckled, we see the emergence of $\ell = 4, 8, \ldots$ modes, typically associated with octahedral symmetry as well as the $\ell = 2$ mode which does not belong to the icosahedral group, tetrahedral group, or the octahedral group. During the snap-through transition, akin to a first order phase transition, the $\ell = 2, 4$ modes are excited as seen from Fig. 3(b) and remain significant even as the pressure is reduced. The W_ℓ's highlight this effect wherein at high external pressure we see the emergence of approximate octahedral symmetry. Indeed, at point 4, we find that $|W_4| = 0.1529$, a value very close to that of the octahedron. Evidently, there is a spontaneous breaking of icosahedral symmetry during this abrupt buckling transition and an emergence of another symmetry group corresponding to a d-wave excitation ($\ell = 2$) mode. We find that $W_2 \approx -0.233$ during the return portion of the hysteresis loop which also exhibits return point memory [30]; i.e., the system returns to the original curve at exactly the same state that it left. The negative value of W_2 indicates a reduced symmetry which is oblate as opposed to prolate, scaling with $Y_2^0 \propto (3\cos^2\theta - 1)$, averaged over all the vertices [31]. Similar effects are seen for the large deformation behavior of other platonic shells (see [14]).

To understand these transitions, we note that for a featureless spherical shell with perfect symmetry, $Q_\ell = \delta_{\ell,0}$. As the shell buckles, some of the a_ℓ^m for $\ell \neq 0$ will become nonzero. A shell with a broken spherical symmetry is characterized by a set of dominant ℓ modes Λ that characterizes the buckled shape

$$\delta D(\theta, \phi) = D(\theta, \phi) - a_0^0 Y_0^0 \approx \sum_{\ell \in \Lambda} \sum_{m=-\ell}^{\ell} a_\ell^m Y_\ell^m(\theta, \phi) + \cdots. \quad (4)$$

This observation allows us to use a Landau-like theory of phase transitions [21,22,32], by writing down a free energy involving rotationally invariant combinations of a_ℓ^m's given by

$$F = \sum_{\ell_i \in \Lambda} F_{\ell_i} + \sum_{\ell_i, \ell_j \in \Lambda, i \neq j} F_{\ell_i, \ell_j} + \cdots, \quad (5)$$

where

$$F_\ell = \alpha_\ell \sum_{m=-\ell}^{\ell} |a_\ell^m|^2 + \beta_\ell \sum_{\Omega} \begin{pmatrix} \ell & \ell & \ell \\ m_1 & m_2 & m_3 \end{pmatrix} a_\ell^{m_1} a_\ell^{m_2} a_\ell^{m_3} \quad (6)$$

and

$$F_{\ell_i, \ell_j} = \gamma_{\ell_i, \ell_j} \sum_{\Omega} \begin{pmatrix} \ell_i & \ell_i & \ell_j \\ m_1 & m_2 & m_3 \end{pmatrix} a_{\ell_i}^{m_1} a_{\ell_i}^{m_2} a_{\ell_j}^{m_3}. \quad (7)$$

Here α_ℓ and β_ℓ are pressure-dependent parameters whose signs determine the order of the shape transition and γ_{ℓ_i, ℓ_j} measures the coupling between the modes ℓ_i and ℓ_j. The presence of the coupling term F_{ℓ_i, ℓ_j} implies that nonzero ℓ_i spherical harmonics can generate ℓ_j modes if these are not already nonzero [33]. This coupling term is unnecessary during the slow deformation phase, but is important during the abrupt collapse phase [see Figs. 3(b) and 3(c)].

During the slow buckling process of the icosahedron shell or dodecahedron shell, a single mode free energy $F = F_6$ suffices; likewise, the slow buckling of the cube shell and octahedron shell can be described by $F = F_4$. If the second-order coupling constant $\alpha_\ell(p)$ becomes nonzero with increasing pressure, then F_ℓ will be minimized by a state such that $a_\ell^m \neq 0$ where the quadratic term in Eq. (6) dominates the free energy. Furthermore, if the third-order coupling constant $\beta_\ell \neq 0$, Landau theory predicts that this will be a first-order transition that leads to hysteresis [21,22,32]. For single mode shape transitions, if we fix the magnitude of Q_ℓ and assume the transition is weakly first order, then the preferred state can be found by minimizing the third order term in Eq. (6), with the second order term held fixed [22]. In general, the form of the transition is determined by finding extrema of the symmetry invariant W_ℓ [22–24]; more details can be found in [14]. However, to understand the full loading cycle, the complete free energy expression as given by Eq. (5) is required.

Our analysis of the buckling process of crystalline shells with different topological defects in the frozen defect limit shows that the number, type, and symmetry of the defects allows us to generate elastic platonic solids. This interplay of topology, geometry, and mechanics suggests a novel way to create polyhedra that differs from previous work [34], where the authors use two-component elastic shells, in contrast to using defects to pattern and drive the faceting transition. The buckling process underlying shape transitions can be understood by studying rotational invariant quantities, which quantifies the symmetry of the structure in terms of a Landau free energy model that captures the symmetry-breaking transition of the shell during the full loading and unloading cycle of the crystalline shell. Our results for athermal shells are naturally applicable to macroscopic shells that are made of discrete elements and suggest a simple way to trigger shape changes between smooth and faceted structures on all scales.

We acknowledge support from Harvard Grants No. MRSEC DMR0820484, No. NSF DMR1005289 (D. R. N.), the Kavli Institute for Nano-bio Science and Technology, and the MacArthur Foundation (L. M.).

*Corresponding author.
lm@seas.harvard.edu

[1] M. Yanagisawa, M. Imai, and T. Taniguchi, Phys. Rev. Lett. **100**, 148102 (2008).
[2] H. Pleiner, Phys. Rev. A **42**, 6060 (1990).
[3] E. Katifori, S. Alben, E. Cerda, D. R. Nelson, and J. Dumials, Proc. Natl. Acad. Sci. U.S.A. **107**, 7635 (2010).
[4] M. Abkarian, A. B. Subramaniam, S.-H. Kim, R. J. Larsen, S.-M. Yang, and H. A. Stone, Phys. Rev. Lett. **99**, 188301 (2007).
[5] L. Mahadevan, R. Bendick, and H. Liang, Tectonics **29**, (2010).
[6] H. S. Seung and D. R. Nelson, Phys. Rev. A **38**, 1005 (1988).
[7] D. L. Caspar and A. Klug, Cold Spring Harbor Symp. Quant. Biol. **27**, 1 (1962).
[8] J. Lidmar, L. Mirny, and D. R. Nelson, Phys. Rev. E **68**, 051910 (2003).
[9] M. Widom, J. Lidmar, and D. R. Nelson, Phys. Rev. E **76**, 031911 (2007).
[10] S. S. Datta, H. C. Shum, and D. A. Weitz, Langmuir **26**, 18 612 (2010).
[11] M. J. Bowick, D. R. Nelson, and A. Travesset, Phys. Rev. B **62**, 8738 (2000).
[12] M. J. Bowick, D. R. Nelson, and H. Shin, Phys. Chem. Chem. Phys. **9**, 6304 (2007).
[13] L. Giomi and M. Bowick, Phys. Rev. B **76**, 054106 (2007).
[14] See Supplemental Material at http://link.aps.org/supplemental/10.1103/PhysRevLett.111.177801 for more information regarding calculation details, numerical methods, and movies.
[15] A. Siber, Phys. Rev. E **73**, 061915 (2006).
[16] L. D. Landau, L. P. Pitaevskii, E. M. Lifshitz, and A. M. Kosevich, *Theory of Elasticity* (Pergamon, New York, 1986), 3rd ed.
[17] T. A. Witten, Rev. Mod. Phys. **79**, 643 (2007).
[18] K. Brakke, Exp. Math. **1**, 141 (1992).
[19] See section on phase space and Figs. 1–3 of the Supplemental Material [14] for additional information.
[20] D. R. Nelson, T. Piran, and S. Weinberg, *Statistical Mechanics of Membranes and Surfaces* (World-Scientific, Singapore, 2004), 2nd ed.
[21] D. R. Nelson and J. Toner, Phys. Rev. B **24**, 363 (1981).
[22] P. J. Steinhardt, D. R. Nelson, and M. Ronchetti, Phys. Rev. B **28**, 784 (1983).
[23] F. H. Busse, J. Fluid Mech. **72**, 67 (1975).
[24] D. H. Sattinger, J. Math. Phys. (N.Y.) **19**, 1720 (1978).
[25] S. Onaka, Philos. Mag. Lett. **86**, 175 (2006).
[26] Note from Table I that the sign of W_ℓ for the smallest ℓ for which W_ℓ is nonzero distinguishes the icosahedron from its dual the dodecahedron and the octahedron from its dual the cube. For the tetrahedron $W_3 = 0$, presumably because this object is self-dual.
[27] H. S. M. Coxeter, *Introduction to Geometry* (Wiley Classics Library, New York, 1999), 2nd ed.
[28] J. W. Hutchinson, J. Appl. Mech. **34**, 49 (1967).
[29] For a $(P, 0) = (16, 0)$ icosadeltahedral shell where we approach the continuum limit, the effect of the hysteresis becomes less apparent and the crushed shell remains a faceted icosahedral-like object.
[30] J. P. Sethna, K. Dahmen, S. Kartha, J. A. Krumhansl, B. W. Roberts, and J. D. Shore, Phys. Rev. Lett. **70**, 3347 (1993).
[31] See, e.g., P. G. de Gennes and J. Prost, *The Physics of Liquid Crystals* (Clarendon, Oxford, 1993).
[32] S. Goshen, D. Mukamel, and S. Shtrikman, Solid State Commun. **9**, 649 (1971).
[33] Note that any discrete triangulation punctuated by a regular array of defects will inevitably lead to small nonzero values of $\{a_\ell^m\}$ with the appropriate symmetry, even though the overall shape is nearly spherical. However, the effect of these small background ordering fields is negligible, in light of the large first-order-like transition displayed in Fig. 3.
[34] G. Vernizzi, R. Sknepnek, and M. O. de la Cruz, Proc. Natl. Acad. Sci. U.S.A. **108**, 4292 (2011).